Multi-AUV Formation Predictive Control Based on CNN-LSTM under Communication Constraints

Juan Li [1,2], Zhenyang Tian [2], Gengshi Zhang [2,*] and Wenbo Li [2]

1   Key Laboratory of Underwater Robot Technology, Harbin Engineering University, Harbin 150001, China; lijuan041@hrbeu.edu.cn
2   College of Intelligent Systems Science and Engineering, Harbin Engineering University, Harbin 150001, China; heu9436@hrbeu.edu.cn (Z.T.); liwenbo049@hrbeu.edu.cn (W.L.)
*   Correspondence: zgengshi@163.com

Abstract: For the problem of hydroacoustic communication constraints in multi-AUV leader follower formation, this paper designs a formation control method combining CNN-LSTM prediction and backstepping sliding mode control. First, a feedback linearization method is used to transform the AUV nonlinear model into a second-order integral model; then, the influence of hydroacoustic communication constraints on the multi-AUV formation control problem is analyzed, and a sliding window-based formation prediction control strategy is designed; for the characteristics of AUV motion trajectory with certain temporal order, the CNN-LSTM prediction model is selected to predict the trajectory state of the leader follower and compensate the effect of communication delay on formation control, and combine the backstepping method and sliding mode control to design the formation controller. Finally, the simulation experimental results show that the proposed CNN-LSTM prediction and backstepping sliding mode control can improve the effect of hydroacoustic communication constraints on formation control.

Keywords: formation control; communication constraints; feedback linearization; CNN-LSTM prediction; backstepping slide control

1. Introduction

With the further exploration of the ocean, Autonomous Underwater Vehicles (AUVs) have started to play an important role in various marine activities, and AUVs are commonly used in tasks such as marine ecosystem detection, underwater inspection and surveillance, and subsea pipeline laying [1–3]. As the complexity of AUV missions increases, the operating environment of AUVs will become more and more complex. Due to constraints, such as the limited energy carried by them, AUVs start to look overwhelmed when facing some more demanding tasks. Therefore, multi-AUV collaboration, information sharing, and joint mission accomplishment have become the new direction of AUV development today. Multi-AUV collaboration can accomplish difficult tasks faster and better for single AUVs, especially in data acquisition [4], target search [5–7] and path planning [8,9], etc. Therefore, multi-AUV collaborative operation is the future development trend of AUVs to deal with complex problems in complex environments.

In the actual application, the multi-AUV formation will inevitably be affected by the actual environment, there will be a communication delay when multi-AUVs communicate with each other, and it takes some time to fuse and calculate the information of each sensor, so the real-time information sharing between multi-AUVs cannot be achieved in the actual application and the multi-AUV formation control will produce large control errors [10,11]. Therefore, the study of multi-AUV formation control under communication delay is helpful to apply the theory to practice and promote the development of multi-AUV formation technology.

For the multi-AUV formation control problem, different authors have proposed different solutions. Kang [12] used fuzzy control theory to coordinate the behavior of multiple AUV members, and the fuzzy control scheme inputs for the leader AUV in a multi-AUV formation were the yaw angle during obstacle avoidance and the yaw angle during target finding maneuvers, and the fuzzy control scheme for the follower consisted of the yaw angle deviations during obstacle avoidance and formation keeping. Borhaug [13] proposed a time-varying smooth feedback control law for multiple non-complete AUVs to maintain formation. An integral backstepping method was used to cooperatively park the follower AUV in its desired docking position and orientation relative to the leader, and the above control law was applied to a real AUV formation system to investigate the implementation problem and singularity avoidance problem of the physical AUV system. Ding [14] proposed a multi-AUV 3D formation control and obstacle avoidance method based on backstepping control and a bio-inspired neural network model. The followers track the virtual AUVs, during which the backstepping control method is guided to achieve 3D underwater formation control. The formation of AUVs was transformed using a bio-neural network model in order to avoid obstacles and pass through the area of obstacles. For the problem of leader failure in multi-AUV leader-following formations, Juan [15] proposed a solution to the problem of leader failure in multi-AUV leader-following formations by using the Hungarian algorithm to reconstruct the failed formation with the lowest cost. The Hungarian algorithm was improved to solve the nonstandard assignment problem. To address the issue of increased leader communication pressure after formation reconstruction, an event trigger mechanism was applied to reduce unnecessary communication. The efficiency of the event trigger mechanism was improved by increasing the event trigger condition of the sampling error threshold. Zheping [10] considered the presence of bounded communication delay and non-convex control input constraints in multi-AUV formation under weak communication conditions. They proposed a formation consistency constrained controller algorithm for discrete-time leaderless multi-AUV systems with dual independent communication topologies by introducing a constraint operator. For the problem of hydroacoustic communication constraints between multiple AUVs, Yuepeng [16] proposed a consensus control algorithm for multi-AUVs combined with the leader-following method under communication time delay, using graph theory to describe the communication topology of multi-AUVs and introducing a hybrid communication topology to accommodate large formation control. The consensus theory was combined with the leader-following method to construct distributed control laws. Suryendu [17] designed a time-lag estimator based on the gradient descent method to estimate the communication delay, and the actual delay was significantly reduced because the time tagging of the leader AUV state packets was avoided in the formulation of the estimator. Shibin [18] investigated the leader-following consistency problem for a multi-intelligent body system with input delays. A distributed state observer was designed to estimate the states of neighbors using the output information between neighboring intelligences, and a consistency algorithm was proposed using the estimated state information. Sufficient conditions for stability were constructed using Lyapunov theory and solved by a set of linear matrix inequalities with iterative parameters.

Based on the above research results, this paper proposes a formation control method combining CNN-LSTM prediction and backstepping sliding mode control. The specific contributions of this paper are summarized as follows:

1. A multi-AUV formation control method combining CNN-LSTM prediction and backstepping sliding mode control is proposed, the stability of the control method is demonstrated, and the effectiveness of the control method is verified by simulation.

2. Combining the advantages of CNN feature extraction, filtering noise and LSTM temporal memory, a CNN-LSTM prediction model is built for predicting the state information of navigators.

3. Applying the feedback linearization method, the AUV nonlinear model is transformed into a second-order integral model, and the controller is designed by combining

the backstepping method and sliding mode control, which improves the robustness of the controller.

2. AUV Nonlinear Model Building and Feedback Linearization

2.1. AUV Nonlinear Model

To study the motion of the AUV, the fixed coordinate system {E} and the motion coordinate system {O} established in this section are shown in Figure 1.
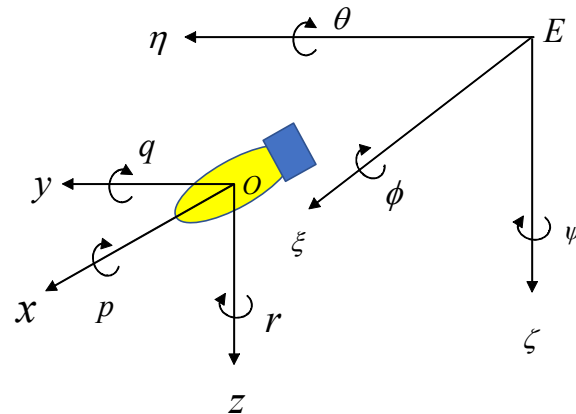
Figure 1. Coordinate system diagram, where $E - \xi\eta\zeta$ is the fixed coordinate system, ξ points due north, η points due east, $O - xyz$ is the motion coordinate system, and O coincides with the center of gravity of the AUV, where the *x*-axis points to the bow of the vehicle.

A fixed point at sea level is usually chosen as the origin of the fixed coordinate system, where the ξ axis points to due north and the η axis points to due east. In order to simplify the nonlinear model of the AUV, the center of gravity of the AUV is chosen as the origin of the motion coordinate system {O}, where the *x* axis is located in the longitudinal mid-profile and points to the bow of the AUV, and the *y* axis is perpendicular to the longitudinal mid-profile and points to the starboard side of the AUV.

In model building, it may be assumed that the AUV studied in this paper is a rigid body with a certain mass distribution, and the effect of its transverse rocking motion is not considered when the AUV is operating underwater, i.e., the transverse rocking attitude angle and angular velocity are kept as desired values. In the following, the nonlinear model of the AUV and the feedback linearization process are based on this assumption.

For the purpose of the following study, the following motion variables are defined:

The position vector in a fixed coordinate system is $\eta = [x \ y \ z \ \theta \ \psi]^T \in R^3 \times S^2$.

The position is $\eta_1 = [x \ y \ z]^T \in R^3$, The attitude angle is $\eta_2 = [\theta \ \psi]^T \in S^2$.

The velocity vector in the motion coordinate system is $v = [u \ v \ w \ q \ r]^T \in R^5$.

The linear velocity in the motion coordinate system is $v_1 = [u \ v \ w]^T \in R^3$.

The angular velocity in the motion coordinate system is $v_2 = [q \ r]^T \in R^2$.

The forces and moments in the motion coordinate system are $T = [X \ Y \ Z \ M \ N]^T \in R^6$.

The force in the motion coordinate system is $T_1 = [X \ Y \ Z]^T \in R^3$.

The moment in the motion coordinate system is $T_2 = [M \ N]^T \in R^2$.

Where R^3 denotes the three-dimensional Euclidean space and S^3 denotes the three-dimensional torus, i.e., there exist three angles in the range $[0, 2\pi]$.

Combining the AUV kinematic model and dynamics model, the AUV nonlinear mathematical model vector expression can be obtained as:

$$\dot{\eta} = J(\eta)v$$
$$M_R\dot{v} + M_A\dot{v} + C_R(v)v + Y(v) + g(\eta) = T + \lambda \tag{1}$$

The kinematic and kinetic mathematical model derivation process and model parameters of the AUV are shown in the literature [19] shown.

2.2. AUV Feedback Linearization Model

As can be seen from Equation (1), the nonlinear model of the AUV is still very complicated even if it is written in vector form. In this subsection, we simplify the AUV nonlinear model by using the transformation method to make the complex problem simple. By coordinate transformation, we can transform the nonlinear model of the AUV in the motion coordinate system to a specific coordinate system, in which the nonlinear model will realize the decoupling of each control channel and transform into a second-order integral model.

According to the literature [20], the AUV model is transformed appropriately:

$$\begin{cases} \dot{\eta} = J(\eta)v \\ \dot{v} = M^{-1}N(\eta,v) + M^{-1}T \end{cases} \tag{2}$$

where $M = M_R + M_A$ is the sum of the inertia matrix and the additional inertia matrix. T denotes the control input forces and moments. Synthesizing the three terms of the model $C_R(v)v, Y(v), g(\eta)$ into a column vector $N(\eta,v)$, then Equation (2) can be transformed into:

$$\begin{bmatrix} \dot{\eta} \\ \dot{v} \end{bmatrix} = \begin{bmatrix} I & 0 \\ 0 & M^{-1} \end{bmatrix} \begin{bmatrix} J(\eta)v \\ N(\eta,v) \end{bmatrix} + \begin{bmatrix} 0 \\ M^{-1} \end{bmatrix} T \tag{3}$$

In Equation (3), a mathematical model with three axial thrusters and two rudders is considered, replacing the controller input T in Equation (3) with the thrust of the axial thrusters $X_{prop}, Y_{prop}, Z_{prop}$ and the rudder angles δ_r, δ_s. The vector $\xi = [\eta^T, v^T]^T$ will be formed by η and v. The two matrices in Equation (3) are taken to be $M_1 = \begin{bmatrix} I & 0 \\ 0 & -M^{-1} \end{bmatrix} \in R^{10 \times 10}$ and $M_2 = \begin{bmatrix} 0 \\ M^{-1} \end{bmatrix} \in R^{10 \times 5}$, respectively. The above Equation (3) is transformed into the following vector form for model linearization:

$$\dot{\xi} = f(\xi) + M_2 g'(\xi)\hat{u} \tag{4}$$

Among them $f(\xi) = M_1 \begin{bmatrix} J(\eta)v \\ N(\eta,v) \end{bmatrix} \in R^{10 \times 1}$, $g'(\xi) = \left[g'_{ij}(\xi) \right] \in R^{5 \times 5}$, $\hat{u} = \left[X_{prop}, Y_{prop}, Z_{prop}, \delta_s, \delta_r \right]^T$.

Vector field: the nonlinear first-order model is taken as the following equation:

$$\begin{aligned} \dot{x} &= f(x) + g(x)u \\ y &= h(x) \end{aligned} \tag{5}$$

where $f(x), g(x), h(x)$ is smooth enough over the definition domain $D \in R^n$, the mapping $f : D \to R^n$ and $g : D \to R^n$ are vector fields over the domain of definition D.

Lie derivative: derivative of y in Equation (5).

$$\dot{y} = \frac{\partial h}{\partial x}[f(x) + g(x)u] = L_f h(x) + L_g h(x)u \tag{6}$$

where $L_f h(x) = \frac{\partial h}{\partial x} f(x)$, $L_g h(x) = \frac{\partial h}{\partial x} g(x)$, is said to be the Lie derivative of h along the smooth vector field f.

Define the output function $\zeta = h(\xi)$, then the dynamics of the AUV are modeled as:

$$\begin{aligned} \dot{\xi} &= f(\xi) + M_2 g'(\xi)\hat{u} \\ \zeta &= h(\xi) \end{aligned} \tag{7}$$

The basic idea of feedback linearization is to find an appropriate coordinate transformation and a control rate after the coordinate transformation.

Select the coordinate transformation $z = \varphi(x)$.

$$
\begin{aligned}
z_1 &= [h_1(x), h_2(x), h_3(x), h_4(x), h_5(x)]^T \\
z_2 &= \left[L_f h_1(x), L_f h_2(x), L_f h_3(x), L_f h_4(x), L_f h_5(x)\right]^T
\end{aligned}
\tag{8}
$$

From transforming the coordinates, we have:

$$
\begin{aligned}
z_1 &= h(x) \\
z_2 &= L_f h(x)
\end{aligned}
\tag{9}
$$

The transformation gives:

$$
\begin{aligned}
\dot{z}_1 &= z_2 \\
\dot{z}_2 &= L_f^2 h(x) + L_g L_f h(\mathrm{x})\hat{u}
\end{aligned}
\tag{10}
$$

In a given coordinate system, to obtain a simpler form, we might as well allow u to equal $L_f^2 h(x) + L_g L_f h(\mathrm{x})\hat{u}$. So, we can obtain the following equation:

$$
u = B(x) + \Gamma(x)\hat{u} = L_f^2 h(x) + L_g L_f h(x)\hat{u}
\tag{11}
$$

Then, the second-order integral model of the AUV in the new coordinate system after transformation can be obtained under the action of Equations (6) and (10).

$$
\hat{u} = \Gamma^{-1}(x)(u - B(x))
\tag{12}
$$

The AUV linearized mathematical model can be obtained as:

$$
\begin{aligned}
\dot{z}_1 &= z_2 \\
\dot{z}_2 &= u
\end{aligned}
\tag{13}
$$

where, z_1 is the position information of the AUV after the coordinate transformation, z_2 is the speed information of the AUV after the coordinate transformation, and u is the control input of the AUV after the coordinate transformation.

3. CNN-LSTM Prediction Model

3.1. Pre-Requisite Knowledge

3.1.1. Convolutional Neural Network

In underwater formations of multiple AUVs, the transmitted track data from the leader to the follower may be subject to both delay and noise interference caused by various factors such as oceanic noise. To enable accurate trajectory prediction, the data must be filtered prior to analysis. In this study, a convolutional neural network is employed to filter the data and extract the relevant trajectory data features. The basic structure diagram of the network is illustrated in Figure 2.
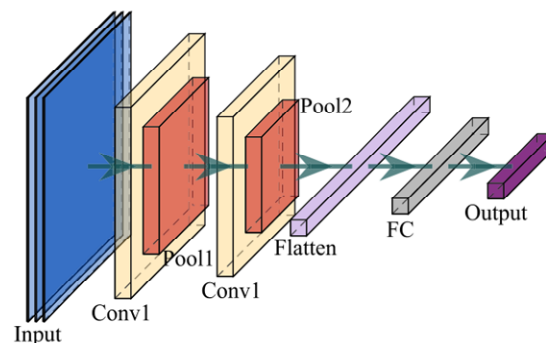

Figure 2. CNN structure schematic.

Figure 2 shows the structure of a convolutional neural network (CNN), which consists of an input layer, a convolutional layer, a ReLU layer, a pooling layer, and a fully connected layer. CNNs differ from traditional neural networks in two main ways:

1. CNNs use a common filter for different regions, which reduces parameters, improves training speed, and prevents overfitting;
2. The output of a CNN is related to only a portion of the input data due to the convolutional layers, which allows for the extraction of exclusive features for each input, whereas a traditional neural network is fully connected and outputs are related to all input units.

3.1.2. Long Short-Term Memory

For problems related to time series, such as AUV formation tracking, traditional neural network algorithms such as CNNs are not fully applicable. Long short-term memory (LSTM) networks are better suited for these problems due to their memory effect. LSTM networks use memory modules instead of traditional storage units, which are interconnected recursive subnetworks. The memory module contains gates that control the flow of information, allowing for memory information to affect neuronal nodes at longer time intervals. The three gates of an LSTM cell are the input gate, output gate, and forgetting gate, which control the storage and inflow of information as well as the core cell unit. The cell structure of LSTM is shown in Figure 3. The activation function plays an important role in the neural network by introducing nonlinear factors into the model, enabling it to perform well on problems where the linear model is not suitable.
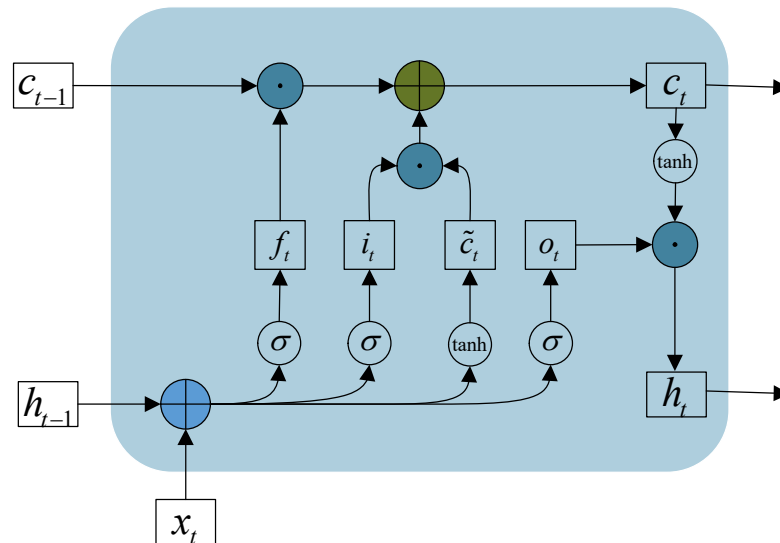

Figure 3. LSTM cell structure diagram.

In Figure 3, the symbol "f_t" represents the forgetting gate, "i_t" represents the input gate, and "o_t" represents the output gate. "x_t" denotes the input to the input layer at time "t", "h_t" denotes the output at time "t", "C_t" denotes the state value of the memory cell at time "t", and "σ" represents the sigmoid function. The mathematical expressions for "σ" and "tanh" in the figure are as follows:

$$\sigma(z) = \frac{1}{1 - e^{-z}} \tag{14}$$

$$\tanh(x) = \frac{e^x - e^{-x}}{e^x + e^{-x}} \tag{15}$$

The LSTM processes the data internally as follows:

$$f_t = \sigma\left(W_{xf}x_t + W_{hj}h_{t-1} + b_f\right) \qquad (16)$$

$$i_t = \sigma(W_{ri}x_t + W_{hi}h_{t-1} + b_i) \qquad (17)$$

$$o_f = \sigma(W_{xv}x_t + W_{hu}h_{t-1} + b_o) \qquad (18)$$

$$c_t = f_t \cdot c_{t-1} + i_t \cdot \tanh(W_{xc}x_t + W_{hc}h_{t-1} + b_c) \qquad (19)$$

$$h_i = o_t \cdot \tanh(c_t) \qquad (20)$$

where, W is the weight matrix, $\cdot$ is the product of point pairs, and b is the deviation.

From Equations (14)–(18), it can be seen that the LSTM is computed by first calculating the values of the forgetting gate, input gate, output gate, and candidate state h_{t-1} and the input at the current moment based on the external state. Next, the internal state c_{t-1} is used to compute the values of the forgetting gate, the input gate and the candidate state in order to update the internal state c_t. Finally, the information is passed to the external state h_t via the current internal state and output gates.

3.2. CNN-LSTM Prediction Model Building

This paper proposes a neural network prediction model that combines the advantages of CNN feature extraction and noise filtering with LSTM temporal memory. The model is designed by connecting the CNN and LSTM layers in series, and its structure is depicted in Figure 4.
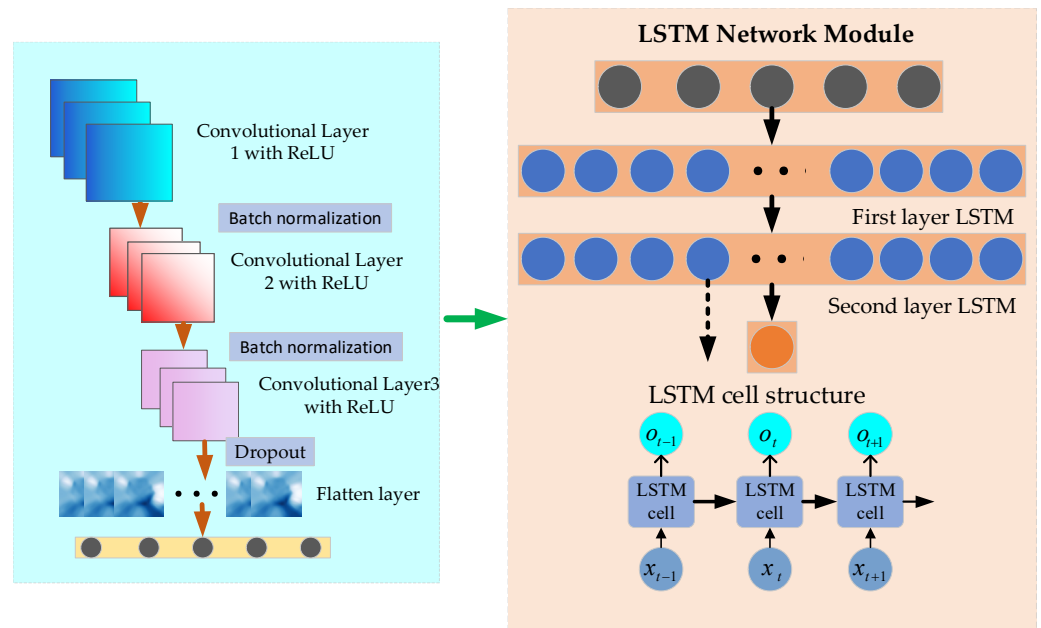

Figure 4. CNN-LSTM prediction model diagram.

The proposed structure is composed of two main modules: the data processing module and the model prediction module. Upon receiving the navigator state information, the data are first preprocessed and then fed into the prediction model. As illustrated in Figure 4, the CNN module is composed of three convolutional layers: a BatchNorm layer, a dropout layer, an expansion layer, and a fully connected layer, which is responsible for receiving the preprocessed data and extracting data features. The LSTM module, on the other hand, consists of two LSTM layers, which analyze the features extracted by the CNN, explore the time series relationships in the data, and predict multiple future points.

The overall prediction process is as follows: the navigator state information is pre-processed by the data processing module, and the processed data are passed to the CNN module for filtering and spatial feature learning. The CNN generates a sequence of high-level features representing the capture and passes it to the tensor processing module. The tensor processing layer then reshapes the output of the CNN so that it can be accepted by the LSTM sub-module. Finally, the LSTM module learns the time-series dependencies of the delayed data and outputs the predicted values for the current moment.

4. Predictive Control of Multi-AUV Formations Based on CNN-LSTM Models

4.1. Multi-AUV Formation Controller Design under Ideal Communication Conditions

It may be assumed that there are five AUVs in the formation: one leader and four followers. The formation that the formation wants to form and maintain is an isosceles triangle (the specific formation is shown in Figure 5 below), and the AUVs are required to maintain the formation even when making a spiral dive.
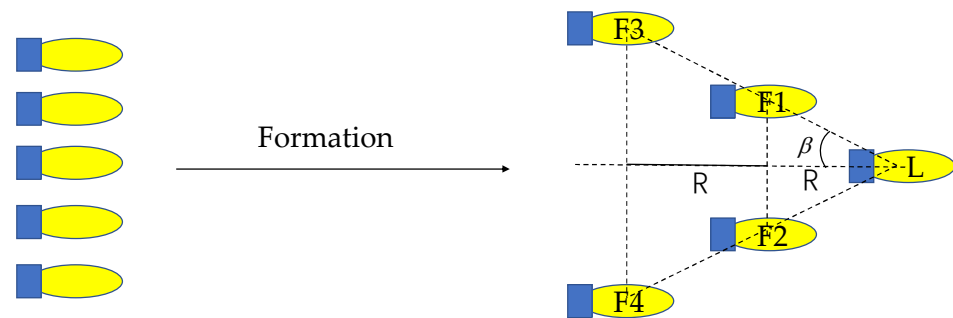

Figure 5. Formation diagram.

As shown in Figure 5, L denotes the leader, and *F1*, *F2*, *F3* and *F4* are all follower AUVs. According to the formation that we want to achieve, we introduce the variables *R* and *β* to constrain the formation, where the distance from the leader to the followers *F1* and *F2* line is *R*, the distance from the follower *F1* and *F2* line to the follower *F3* and *F4* line is also *R*, and the attitude angle of the formation hold is *β*. The formation constraints proposed in this paper are:

$$
\begin{cases}
\eta_{F1} + d_1 = \eta_L \\
\eta_{F2} + d_2 = \eta_L \\
\eta_{F3} + d_3 = \eta_L \\
\eta_{F4} + d_4 = \eta_L
\end{cases}
$$
$$
\begin{cases}
\dot{\eta}_{F1} + dv_1 = \dot{\eta}_L \\
\dot{\eta}_{F2} + dv_2 = \dot{\eta}_L \\
\dot{\eta}_{F3} + dv_3 = \dot{\eta}_L \\
\dot{\eta}_{F4} + dv_4 = \dot{\eta}_L
\end{cases}
\tag{21}
$$

where d_1, d_2, d_3, d_4, dv_1, dv_2, dv_3 and dv_4 are denoted as:

$$
\begin{cases}
d_1 = (-(\cos\beta)^{-1} R\cos(\psi_L - \beta - \frac{\pi}{2}), (\cos\beta)^{-1} R\cos(\psi_L + \beta - \frac{\pi}{2}), 0, 0, 0)^T \\
d_2 = (-(\cos\beta)^{-1} R\cos(\psi_L + \beta - \frac{\pi}{2}), -(\cos\beta)^{-1} R\cos(\psi_L - \beta - \frac{\pi}{2}), 0, 0, 0)^T \\
d_3 = (-(\cos\beta)^{-1} 2R\cos(\psi_L - \beta - \frac{\pi}{2}), (\cos\beta)^{-1} 2R\cos(\psi_L + \beta - \frac{\pi}{2}), 0, 0, 0)^T \\
d_4 = (-(\cos\beta)^{-1} 2R\cos(\psi_L + \beta - \frac{\pi}{2}), -(\cos\beta)^{-1} 2R\cos(\psi_L - \beta - \frac{\pi}{2}), 0, 0, 0)^T
\end{cases}
$$
$$
\begin{cases}
dv_1 = J_\eta (r_L \tan(-\beta) \times R, 0, 0, 0, 0)^T \\
dv_2 = J_\eta (r_L \tan(\beta) \times R, 0, 0, 0, 0)^T \\
dv_3 = J_\eta (r_L \tan(-\beta) \times 2R, 0, 0, 0, 0)^T \\
dv_4 = J_\eta (r_L \tan(\beta) \times 2R, 0, 0, 0, 0)^T
\end{cases}
\tag{22}
$$

In a leader-follower formation control with five AUVs, the motion state vector of the *i* th follower AUV at the moment of *t* is $\varepsilon_i(t) = \eta_i(t)$ and the motion state vector of the

leader is $\varepsilon_L(t) = \eta_L(t)$. If the formation satisfies Equation (23), it is said that the formation can achieve formation maintenance and stability convergence.

$$\begin{aligned} \lim_{t\to\infty}\left|\varepsilon_i(t) - \varepsilon_L(t) + d_i\right| &= 0 \\ \lim_{t\to\infty}\left|\dot{\varepsilon}_i(t) - \dot{\varepsilon}_L(t) + dv_i\right| &= 0 \end{aligned} \qquad i = 1,2,3,4 \qquad (23)$$

Let the attitude vector of the i th follower AUV at the time of t and the attitude vector of the leader AUV at the time of z_{1d} in the lead follower formation control of the AUV be z_{1i}.

Define the trajectory tracking error of the i th follower AUV as $z_{i1e} = z_{i1} - z_{1d} + d_i$, then $\dot{z}_{i1e} = z_{i2} - \dot{z}_{1d}$.

Define the following Lyapunov function:

$$V_{i1} = \frac{1}{2}z_{i1e}{}^2 \qquad (24)$$

Define $z_{i2} = z_{i2e} + \dot{z}_{1d} - c_{i1}z_{i1e}$, where c_{i1} is the positive constant and z_{i2e} is the intermediate virtual control item. We can get $z_{i2e} = z_{i2} - \dot{z}_{1d} + c_{i1}z_{i1e}$, and the derivation gives $\dot{z}_{i1e} = z_{i2} - \dot{z}_{i1d} = z_{i2e} - c_{i1}z_{i1e}$.

The derivative of V_{i1} gives:

$$\dot{V}_{i1} = z_{i1e}\dot{z}_{i1e} = z_{i1e}z_{i2e} - c_{i1}z_{i1}{}^2 \qquad (25)$$

Define the switching function as:

$$\sigma_i = k_{i1}z_{i1e} + z_{i2e} \qquad (26)$$

Among them, $k_{i1} > 0$.

Because of $\dot{z}_{i1e} = z_{i2e} - c_{i1}z_{i1e}$, we can derive:

$$\sigma_i = k_{i1}z_{i1e} + z_{i2e} = k_{i1}z_{i1e} + \dot{z}_{i1e} + c_{i1}z_{i1e} = (k_{i1} + c_{i1})z_{i1e} + \dot{z}_{i1e} \qquad (27)$$

Because of $k_{i1} + c_{i1} > 0$, there is $\sigma_i = 0$ only when $z_{i1e} = 0$, $z_{i2e} = 0$ and $\dot{V}_{i1} \leq 0$. For this, the next design step is needed.

Define the following Lyapunov function.

$$V_{i2} = V_{i1} + \frac{1}{2}\sigma_i{}^2 \qquad (28)$$

The derivative of V_{i2} gives:

$$\begin{aligned} \dot{V}_2 &= \dot{V}_{i1} + \sigma_i\dot{\sigma}_i \\ &= z_{i1e}z_{i2e} - c_{i1}z_{i1e}{}^2 + \sigma_i\dot{\sigma}_i \\ &= z_{i1e}z_{i2e} - c_{i1}z_{i1e}{}^2 + \sigma_i(k_{i1}\dot{z}_{i1e} + \dot{z}_{i2e}) \\ &= z_{i1e}z_{i2e} - c_{i1}z_{i1e}{}^2 + \sigma_i(k_{i1}(z_{i2e} - c_{i1}z_{i1e}) + \dot{z}_{i2} - \ddot{z}_{1d} + c_{i1}\dot{z}_{i1e}) \\ &= z_{i1e}z_{i2e} - c_{i1}z_{i1e}{}^2 + \sigma_i(k_{i1}(z_{i2e} - c_{i1}z_{i1e}) + U_i + F - \ddot{z}_{1d} + c_{i1}\dot{z}_{i1e}) \end{aligned} \qquad (29)$$

where U_i is the expression of the controller to be designed. F is the total uncertainty of the system.

The design of the i follower controller is shown below.

$$U_i = -k_{i1}(z_{i2e} - c_{i1}z_{i1e}) - \bar{F}\tanh(\sigma_i) + \ddot{z}_{1d} - c_{i1}\dot{z}_{i1e} - h_i(\sigma_i + \beta_i\tanh(\sigma_i)) \qquad (30)$$

where h_i and β_i are positive constants.

Substituting Equation (30) into $\dot{V}_{i2}$ yields:

$$
\begin{aligned}
\dot{V}_{i2} &= z_{i1e}z_{i2e} - c_{i1}z_{i1e}{}^2 - h_i\sigma_i{}^2 - h_i\beta_i|\sigma_i| + F\sigma_i - \overline{F}\sigma_i \\
&\leq -c_{i1}z_{i1e}{}^2 + z_{i1e}z_{i2e} - h_i\sigma_i{}^2 - h_i\beta_i|\sigma_i|
\end{aligned}
\tag{31}
$$

Let Q_i be equal to the following matrix.

$$
Q_i = \begin{bmatrix} c_{i1} + h_i k_{i1}^2 & h_i k_{i1} - \frac{1}{2} \\ h_i k_{i1} - \frac{1}{2} & h_i \end{bmatrix}
\tag{32}
$$

Due to

$$
\begin{aligned}
z_{ie}{}^{\mathrm{T}}Q_i z_{ie} &= \begin{bmatrix} z_{i1e} & z_{i2e} \end{bmatrix} \begin{bmatrix} c_{i1} + h_i k_{i1}^2 & h_i k_{i1} - \frac{1}{2} \\ h_i k_{i1} - \frac{1}{2} & h_i \end{bmatrix} \begin{bmatrix} z_{i1e} & z_{i2e} \end{bmatrix}^{\mathrm{T}} \\
&= c_{i1}z_{i1e}^2 - z_{i1e}z_{i2e} + h_i k_{i1}^2 z_{i1e}^2 + 2h_i k_{i1}z_{i1e}z_{i2e} + h_i z_{i2e}^2 \\
&= c_{i1}z_{i1e}^2 - z_{i1e}z_{i2e} + h_i\sigma_i^2
\end{aligned}
\tag{33}
$$

Among them, $z_{ie}{}^T = \begin{bmatrix} z_{i1e} & z_{i2e} \end{bmatrix}$.
If you want to guarantee that Q_i is a positive definite matrix, then

$$
\dot{V}_{i2} = -z_{ie}{}^{\mathrm{T}}Q_i z_{ie} - h_i\beta_i\left|\sigma_i\right| \leqslant 0
\tag{34}
$$

Due to

$$
\left| Q_i \right| = h_i\left(c_{i1} + h_i k_{i1}^2\right) - \left(h_i k_{i1} - \frac{1}{2}\right)^2 = h_i(c_{i1} + k_{i1}) - \frac{1}{4}
\tag{35}
$$

Therefore, it is possible to guarantee $\dot{V}_{i2} \leq 0$ by taking the values of h_i, c_{i1} and k_{i1} such that $|Q_i| > 0$, i.e., Q_i is a positive definite matrix.

By taking the values of h, c_1 and k_1, you can make $|Q| > 0$. Thus, it can be deduced that Q is a positive definite matrix and that $\dot{V}_2 \leq 0$ is guaranteed.

According to LaSalle's invariance principle, when $\dot{V}_{i2} \equiv 0$ is taken, it can be deduced that $z_{ie} \equiv 0$, $\sigma_i \equiv 0$. When $t \to \infty$, since $z_{i1e} \to 0$, $z_{i2e} \to 0$, it can be deduced that $z_{i2e} \to 0$, $\dot{z}_{i1} \to \dot{z}_{1d}$.

In summary, it can be seen that the Lyapunov functions V_{i1} and V_{i2} are positive definite, and the values of V_{i1}, c_{i1} and k_{i1} can be reasonably chosen to ensure that $\dot{V}_{i1}$ and $\dot{V}_{i2}$ are negative definite, so the designed AUV formation controller (30) is stable and convergent.

4.2. Sliding Window-Based Predictive Control of Multi-AUV Formations under Communication Constraints

In the previous section, the backstepping sliding mode control method was used and the formation controller was designed according to the formation constraint relationship. The controller for the follower AUV in the formation with time-lag state is presented below due to the communication delay between the leader and the follower and the limitations of the hydroacoustic sonar in transmitting high-frequency signals, resulting in a longer communication interval between them. As a consequence, the follower may not receive the real-time status information of the leader.

$$
U_i = -k_{i1}(z_{i2e} - c_1 z_{i1e}) - \overline{F}\tanh(\sigma_i) + \ddot{z}_{1d} - c_1\dot{z}_{i1e} - h(\sigma_i + \beta\tanh(\sigma_i))
\tag{36}
$$

where, $z_{i1e} = z_{i1} - z_{1d}(t - \tau) + d_i$, $z_{i2e} = z_{i2} - z_{2d}(t - \tau) + c_1 z_{i1e} + dv_i$, $\sigma_i = k_1 z_{i1e} + z_{i2e}$, and τ are the communication delay times between the navigator and the follower.

To illustrate the effect of communication delay on formation control while preparing for a new predictive control strategy, the following assumptions are made about the

communication delay between the leader and the follower and the hydroacoustic sonar occurrence interval:

Assumption 1. *The distance between the navigator and the follower is close, and the speed of acoustic wave transmission in the water is 1500 m/s, so the communication time delay caused by the communication transmission is small, where it is assumed that the delay time between the broadcast of the navigator sending the status information and the follower receiving the information and measuring the settlement is 1 s.*

Assumption 2. *Due to the limitation of communication bandwidth, the navigator cannot send too many beats of historical status data to the follower at one time; so, suppose the navigator can send five beats of status data to the follower at one time.*

Assumption 3. *The hydroacoustic sonar is unable to sound at high frequencies and the sounding time is affected by the size of the data sent, assuming that the communication interval of the hydroacoustic sonar is 6–9 s.*

To solve the communication delay and communication interval problem between the leader and the follower, this section proposes a formation control strategy based on a sliding window to achieve multi-step prediction, which iterates the historical state information of the leader to predict the current state information of the leader step by step, which saves computational efficiency and has better adaptability compared with the observer-based iterative prediction method. The specific principle of the strategy is described below.

At the M time, the navigator sends its own status data $\{Z_1, Z_2, \cdots\cdots Z_{M-1}, Z_M\}$ from the previous M time to the follower in the formation. Due to the communication transmission delay τ_{tran} and the hydroacoustic sonar sounding time consuming τ_{inter}, a fixed time delay $\tau_{once\_tal} = \tau_{tran} + \tau_{inter}$ is defined, and the follower receives the status information of the navigator at the $M + \tau_{once\_tal}$ time, and the status information of the navigator received by the follower at this time is the status information of the navigator at the M time. So, the follower needs to predict the state information of the leader at the $M + \tau_{once\_tal}$ time as the tracking target based on the state information of the leader at the M time.

The second sounding of the sonar starts immediately after the first sounding. Since the transmission delay after the first sounding is included in the second sonar sounding elapsed time, the follower needs time τ_{inter} to receive the information of the navigator for the second time. Therefore, after the follower receives the status information of the navigator at the $M + \tau_{once\_tal}$ time, the follower firstly has to predict the status information of the navigator at the M time as the tracking target; secondly, since the follower cannot receive the status information of the navigator at the τ_{inter} time in the future, the follower needs to then predict the status information of the navigator at the τ_{inter} time in the future. A schematic diagram of the information transfer process is shown in Figure 6.
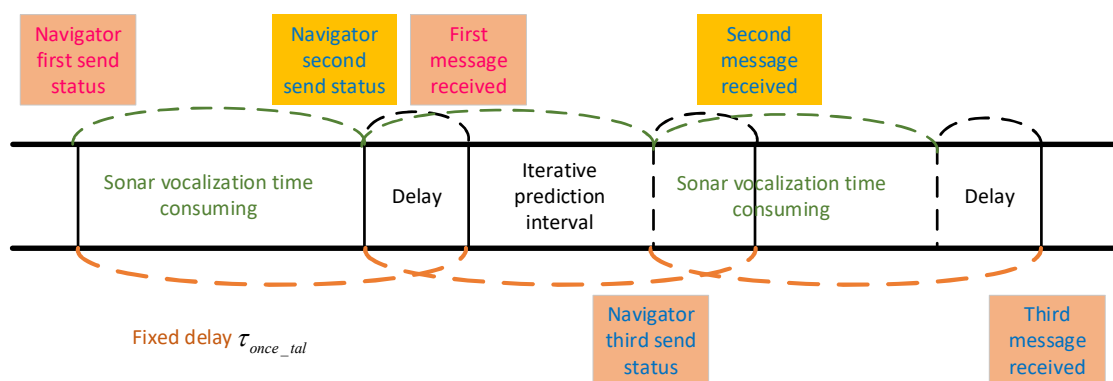

Figure 6. Information transmission diagram.

This paper focuses on predicting the real-time state of the leader in AUV formation by using delayed state data received by the followers as input to the prediction model. The delayed data are in the form of a time series, and to achieve continuous prediction, a sliding window approach is designed where the delay information is fed into the window as input and the real information as output, as illustrated in Figure 7. To evaluate the model's performance, a delay time of 10 s is set, and the size of the sliding window, which corresponds to the time step of the input data, is set to 5. The prediction equation is given as follows:

$$z(t) = f(\{z(t-14), \cdots, z(t-11), z(t-10)\}) \tag{37}$$

where $z = [z_1, z_2]$ denotes the position vector of the navigator in time. $z_1 = [x, y, depth, \theta, \psi]^T$, where x, y and $depth$ represent the displacement in three coordinate directions; θ and ψ represent the pitch and heading angles. $z_2 = [u, v, w, q, r]^T$, where u, v and w are the longitudinal, lateral and vertical velocities respectively; q and r are the longitudinal and bow angular velocities.
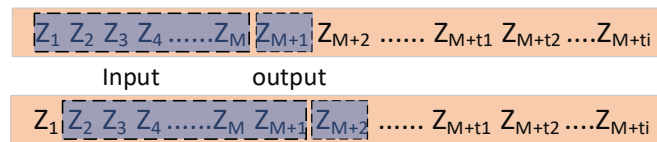

Figure 7. Schematic diagram of the sliding window.

The prediction strategy designed in this paper has two main phases: fixed delay prediction and communication interval prediction. In the fixed delay prediction stage, the follower puts the state information sent by the navigator into the designed sliding window and uses the prediction model to predict the state quantity $\hat{Z}_{M+1}$ at the $M+1$ th time based on the data in the first M times of the sliding window. Put $\hat{Z}_{M+1}$ into the sliding window, and then the sliding window moves forward to obtain $\hat{Z}_{M+2}$ using $\hat{Z}_{M+1}$ and the historical state quantity prediction, and finally obtain the state prediction $\hat{Z}_{M+\tau_{once\_tal}}$ at $M+\tau_{once\_tal}$ moments through continuous iterative prediction.

At the same time, due to the effect of hydroacoustic sonar sounding time consumption, the follower will only receive the next status data from the navigator at the moment of $M+\tau_{once\_tal}+\tau_{inter}$, so the follower will continue to make iterative predictions based on the status quantity $\hat{Z}_{M+\tau_{once\_tal}}$ obtained from the prediction compensation during this period, obtain $\hat{Z}_{M+\tau_{once\_tal}+1+1}$, $\hat{Z}_{M+\tau_{once\_tal}+2} \cdots \cdots \hat{Z}_{M+\tau_{once\_tal}+\tau_{inter}}$, and output in turn until it receives the time delay status data from the navigator again. Based on the above strategy, the follower will get the predicted value of the current moment of the leader; the controller of the follower in the AUV formation at this time is shown below.

$$U_i = -k_{i1}(\hat{z}_{i2e} - c_1\hat{z}_{i1e}) - \overline{F}\tanh(\hat{\sigma}_i) + \ddot{z}_{1d} - c_1\dot{\hat{z}}_{i1e} - h(\hat{\sigma}_i + \beta\tanh(\hat{\sigma}_i)) \tag{38}$$

where, $\hat{z}_{i1e} = z_{i1} - \hat{z}_{1d}(t) + d_i$, $\hat{z}_{i2e} = z_{i2} - \hat{z}_{2d}(t) + c_1\hat{z}_{i1e} + dv_2$, $\hat{\sigma}_i = k_1\hat{z}_{i1e} + \hat{z}_{i2e}$, $\hat{z}_{1d}(t)$ and $\hat{z}_{1d}(t)$ are the predicted values of CNN-LSTM model.

The block diagram of CNN-LSTN-based multi-AUV formation prediction control under communication constraints is shown in Figure 8. Based on the pilot-follower formation control strategy, there is a communication delay when the follower AUV receives the position and speed information from the pilot due to the influence of hydroacoustic communication. In this paper, a CNN-LSTM prediction model is established to make predictions based on the historical information of the pilot, which can well offset the effects of noise and communication delay on formation control. The prediction information and feedback information are used as the input of the AUV formation controller to finally realize the AUV formation prediction control.
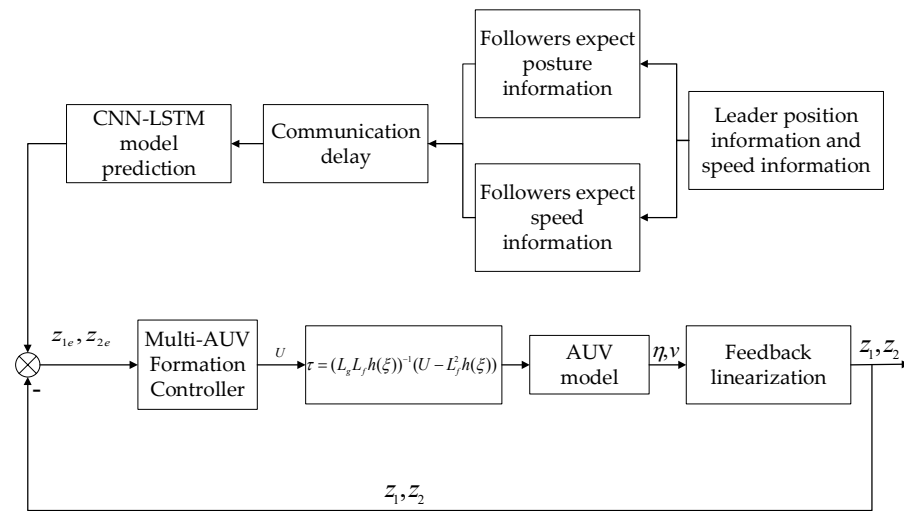
Figure 8. AUV formation prediction control block diagram.

5. Simulation Verification and Analysis

5.1. Simulation Results and Analysis of CNN-LSTM Model

The trajectory data of a small AUV, consisting of longitude and latitude measurements from multiple positioning systems, as well as values from GPS, bathymetry, and Doppler measurements with a maximum depth of 20 m, were selected as the training set for this study. The relevant information of the training set is shown in Table 1.

Table 1. AUV status information.

Sample Size	Maximum Depth (m)	Lon	Lat	U (m/s)
39,875	20	119.18° E	29.56° N	1–3

These training data were obtained from the trajectory data of an AUV on-lake experiment, and some of its trajectories are shown in Figure 9. The raw data were preprocessed and used for the training of the CNN-LSTM model.
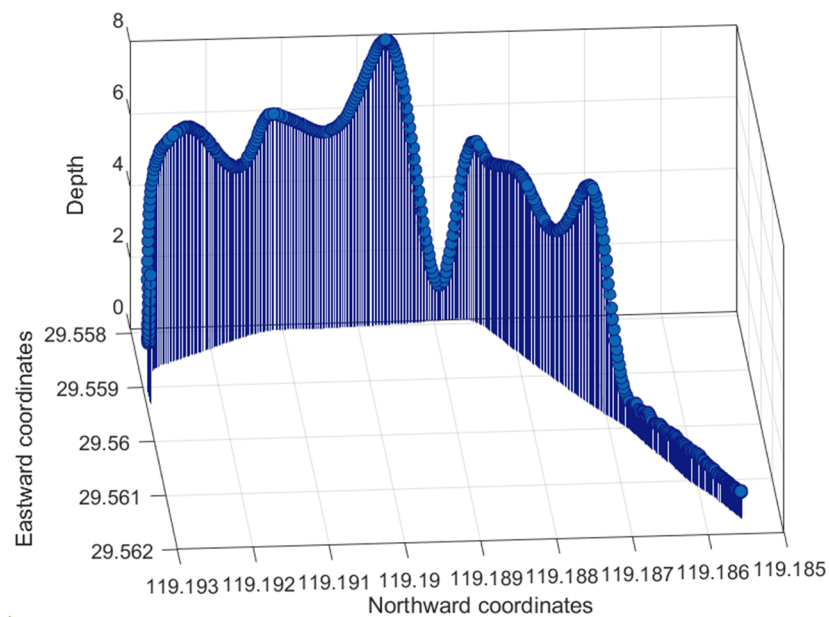
Figure 9. AUV partial trajectory data.

The CNN model designed in this paper contains three convolutional layers with filter sizes of (2, 1), (3, 1) and (3, 1) for each layer, and a dropout layer is added to prevent overfitting. The processed features were passed to the two-layer LSTM model, and the predicted data were output by the last LSTM layer. Through continuous debugging, it was found that the network with 125 and 128 neurons in each layer was trained well. Additionally, to prevent the overfitting of the network, a discard layer with probability 0.3 is built after the hidden layer. The Adam algorithm is used for optimization, and the design learning rate decline period is 100, the learning rate is 0.012, the learning rate decline coefficient is 0.8, and finally, the gradient threshold is set to 1 in order to prevent gradient explosion.

After processing the delayed data according to the aforementioned data processing steps, they are fed into the CNN-LSTM model using the sliding window format. The performance of the model is then evaluated by computing the mean square error (*MSE*) and maximum absolute error (MAXERR) between the predicted values and the actual trajectory data. The evaluation metrics can be formulated as follows:

$$MSE = \frac{1}{N}\sum_{t=1}^{N}(\text{ observed }_t - \text{ predicted }_i)^2 \tag{39}$$

where N indicates the number of samples.

$$\text{Maxerr } = \max\left|\frac{\text{observed}_t - \text{predicted }_t}{\text{observed}}\right| \tag{40}$$

According to Assumption 2, the leader broadcasts the data of the past five beats to each follower at a time, so the size of the sliding window is set to 5, and the prediction effect of the prediction model is verified under the fixed delay of 2 s and the communication interval of 7 s. The selected navigator trajectory is a spiral dive trajectory, and Gaussian white noise with an amplitude of 0.003 is superimposed on the trajectory data, and the LSTM prediction model is selected for simulation comparison. The parameters of the two model designs are shown in Table 2.

Table 2. AUV status information.

Models	Structural Layer	Parameter Setting	Learning Rate
LSTM model	Hidden layer neurons	[10, 10, 10, 10]	0.02
	activation function	ReLU	
	Optimizers	Adam	
	Epochs	30	
	Batch size	128	
CNN-LSTM model	Filter 1	×16 size (2, 1)	0.012
	Filter 2	×16 size (3, 1)	
	Filter 3	×16 size (3, 1)	
	Dropout ratio	0.3	
	Optimizers	Adam	
	LSTM cells 1	10	
	LSTM cells 2	10	
	Activation function	ReLU	

Since the velocity quantities in the selected trajectories are kept constant, in order to objectively compare the advantages and disadvantages of the two prediction models, only the navigator state quantities $z = [x, y, depth, \theta, \psi]$ are compared for prediction, and the simulation results are shown in Figure 10.
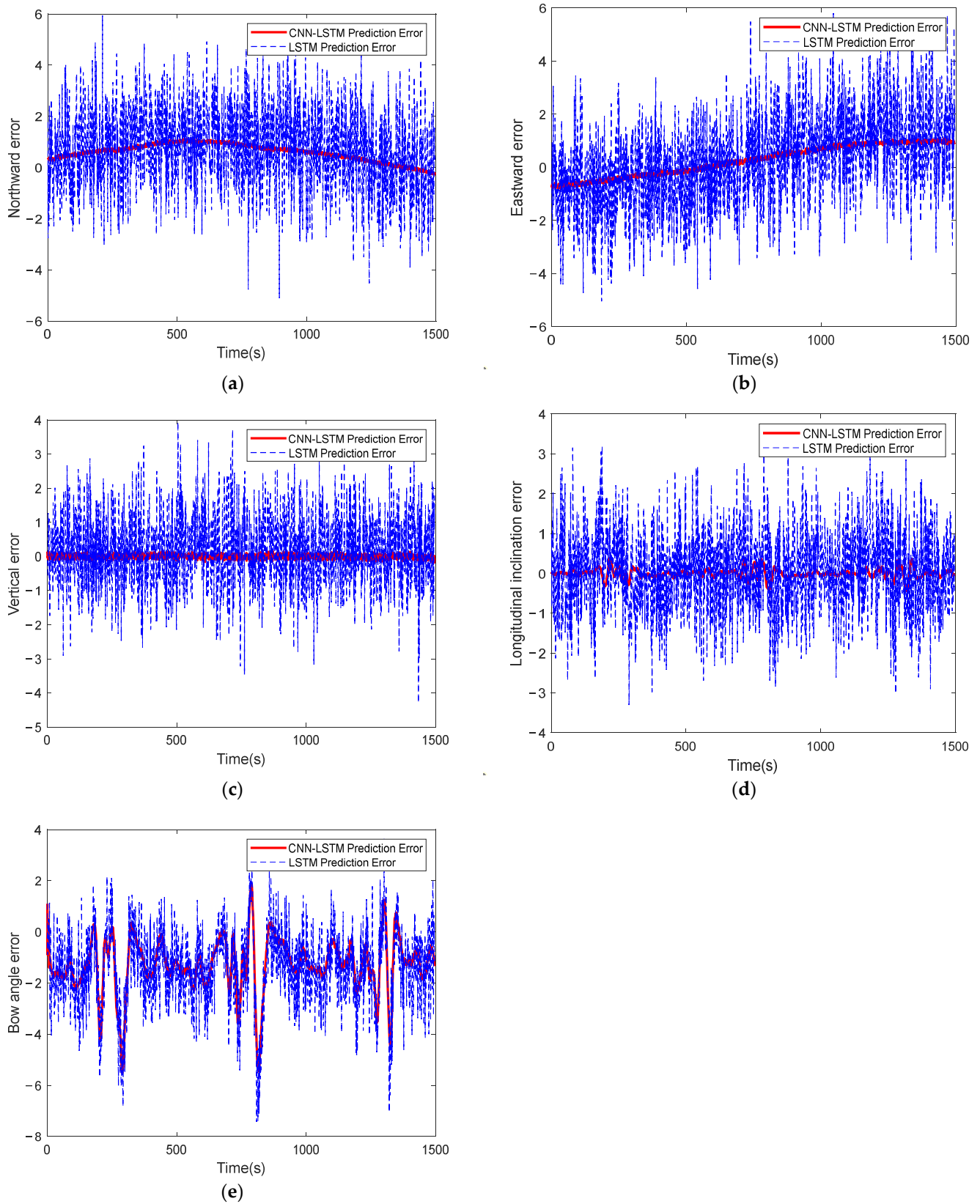
Figure 10. AUV trajectory prediction error: (**a**) northward trajectory prediction error, (**b**) eastward trajectory prediction error, (**c**) vertical trajectory prediction error, (**d**) longitudinal inclination angle prediction error and (**e**) bow angle prediction error.

Based on Figures 10 and 11, it can be observed that the CNN-LSTM model predicts a trajectory that is closer to the actual value, with a smoother prediction curve and lower error fluctuations. These results demonstrate that the CNN-LSTM model provides higher accuracy and stability. The *MSE* values for the predicted states by the LSTM model are 1.7911, 1.7947, 1.1921, 1.6871, and 0.2564, while the CNN-LSTM model predicts the state with lower *MSE* values of 0.6868, 0.6315, 0.0664, 1.3078, and 0.1139. These *MSE* values are smaller compared to those of the pure LSTM model, indicating that the CNN-LSTM model provides better prediction results.
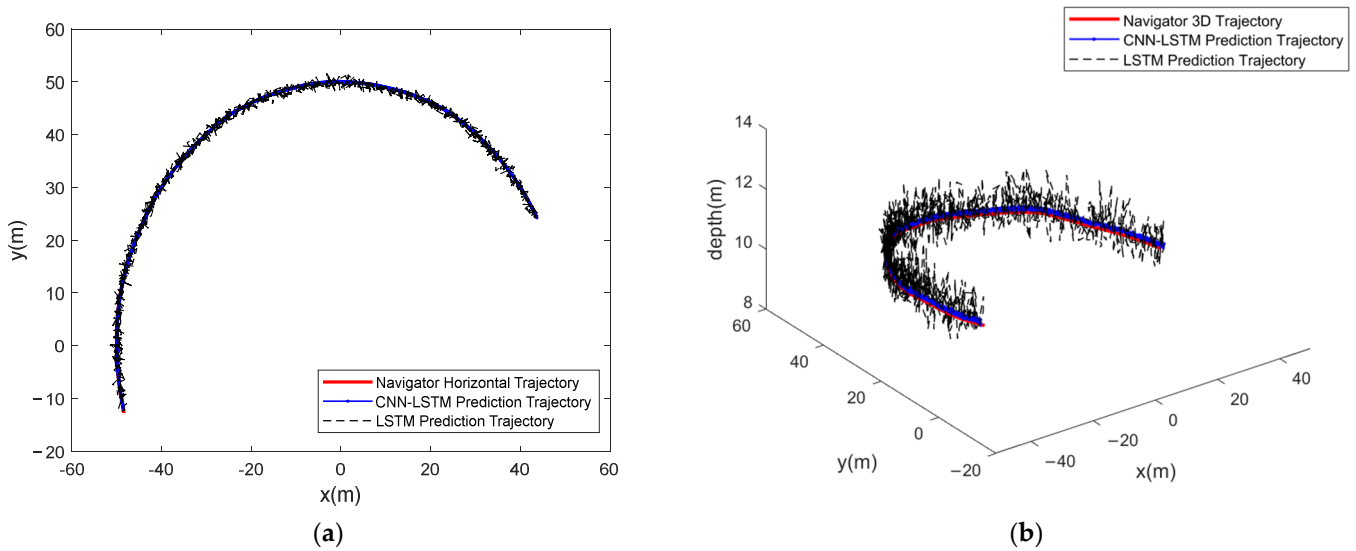
Figure 11. AUV trajectory prediction: (**a**) horizontal plane trajectory prediction and (**b**) 3D trajectory prediction.

5.2. Formatting of Mathematical Components

To verify the prediction effectiveness of the CNN-LSTM prediction model in the formation and formation holding phases of the multi-AUV formation, the communication transmission delay τ_{tran} is set to 1 s and the hydroacoustic sonar sounding delay τ_{inter} is set to 4 s, i.e., the fixed time delay τ_{once_tal} is defined to be 5 s and the maximum total time delay is 9 s. The formation design is consistent with Figure 5.

The navigational track of the navigator is

$$\begin{cases} x_p = 60\cos(2\pi t/1000) \\ y_p = 60\sin(2\pi t/1000) \qquad 0 \le t \le 2000 \\ z_p = -0.3t \end{cases} \tag{41}$$

The initial state of the AUV is as follows: initial position $x(0)$ is randomly taken in the range of [55, 65] m, $y(0)$ is randomly taken in the range of [−10, 10] m, $x(0)$ is 65 m, depth is 0 m, initial attitude $\theta(0)$ is 0 rad, bow angle $\psi(0)$ is $4\pi/3$ rad, longitudinal velocity $u(0)$ is 0.5 m/s, all other velocities are initialized to 0 m/s, and controller parameters are $h = 1$, $k_1 = 0.3$, $c_1 = 0.3$, $F = 0.02$, $\beta = 0.5$.

The simulation results are shown in Figures 12 and 13.

In Figure 12, (a) to (e) are the simulation plots of AUV formation position information, from which it can be seen that the leader and the follower always keep the same position, pitch angle and bow angle during the spiral dive under the action of the formation controller; (f) to (j) are the simulation plots of AUV formation speed information, from which it can be seen that the bow speed, lateral speed and vertical speed of the follower in the formation have some fluctuations, but the overall velocity remains stable. Figure 13 shows the 3D trajectory of the AUV formation and its projection on the horizontal plane, from which it can be seen that the followers can follow the leader more accurately and can realize

the multi-AUV formation control in a 3D environment. The simulation results illustrate that the formation control method combining CNN-LSTM prediction and backstepping sliding mode control designed in this paper can better realize the three-dimensional predictive control of multi-AUV formation under the communication constraints.
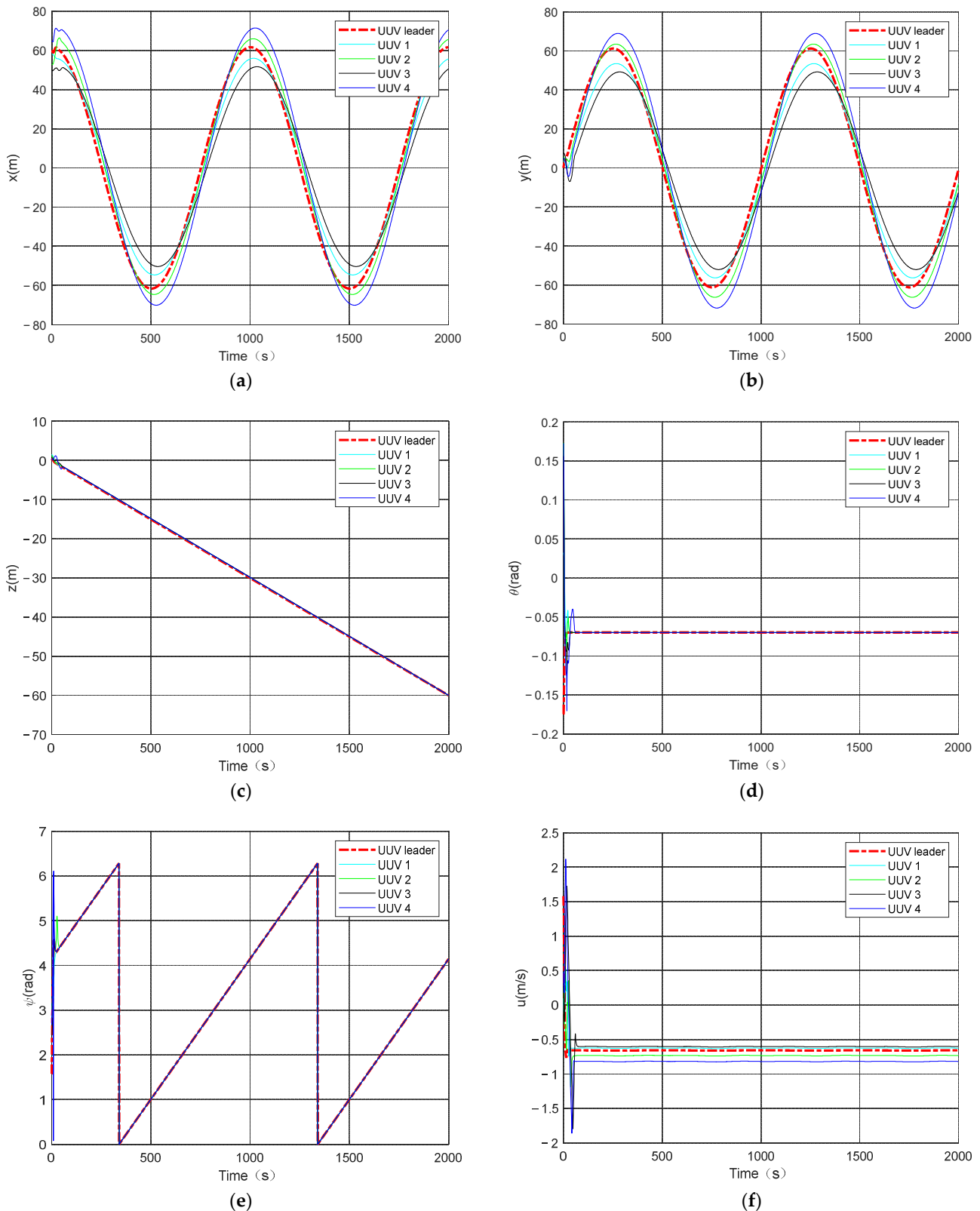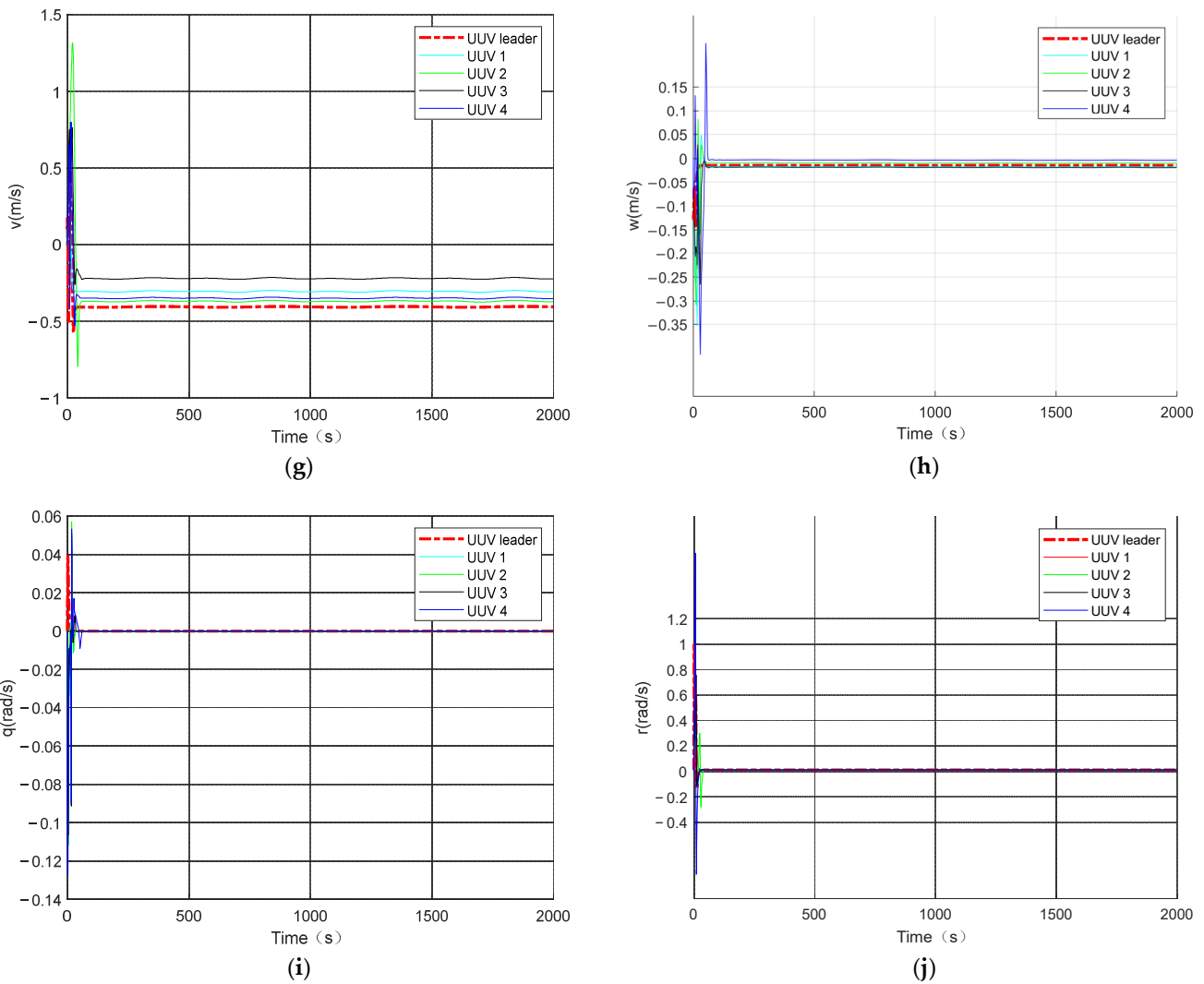

(a)

(b)

(c)

(d)

(e)

(f)

Figure 12. *Cont.*

Figure 12. Simulation diagrams of formation position and velocity information: (**a**) AUV northward trajectory, (**b**) AUV eastward trajectory, (**c**) AUV vertical trajectory, (**d**) AUV longitudinal inclination angle state, (**e**) AUV bow angle state, (**f**) AUV longitudinal velocity, (**g**) AUV lateral velocity, (**h**) AUV vertical velocity, (**i**) AUV longitudinal inclination angle velocity and (**j**) AUV bow angle velocity.
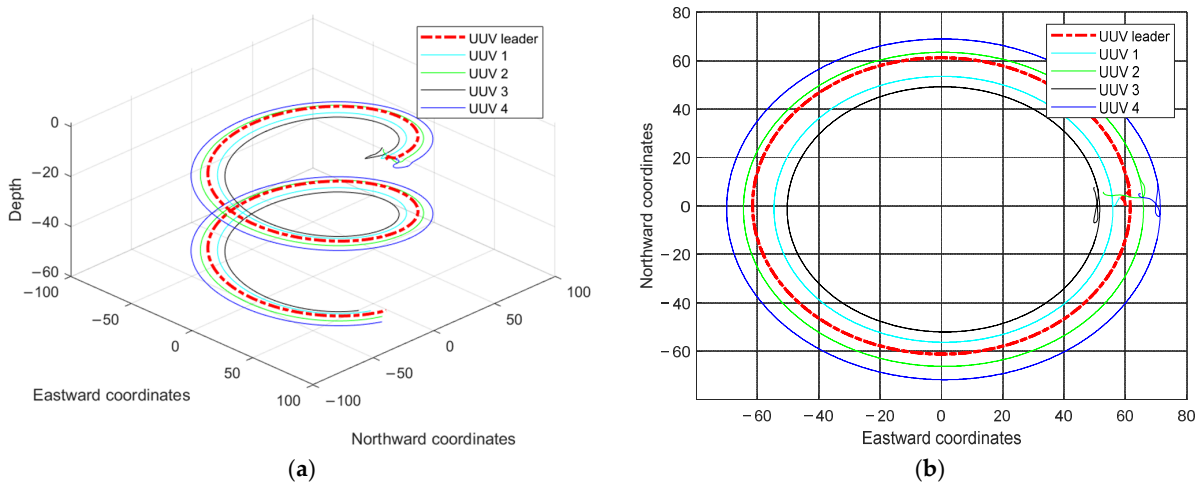
Figure 13. AUV formation 3D trajectory diagram and its horizontal projection: (**a**) 3D trajectory diagram and (**b**) horizontal projection diagram.

Figure 14 shows the position and attitude errors of the AUV formation under CNN-LSTM prediction. Figure 15 shows the position and attitude error of AUV formation under communication delay. From Figures 14a,b and 15a,b, it can be seen that the northward and eastward errors of the AUV formation under predictive control are much smaller than the control errors under delay, indicating that the CNN-LSTM prediction-based AUV formation control method can better overcome the effect of communication delay on formation control.
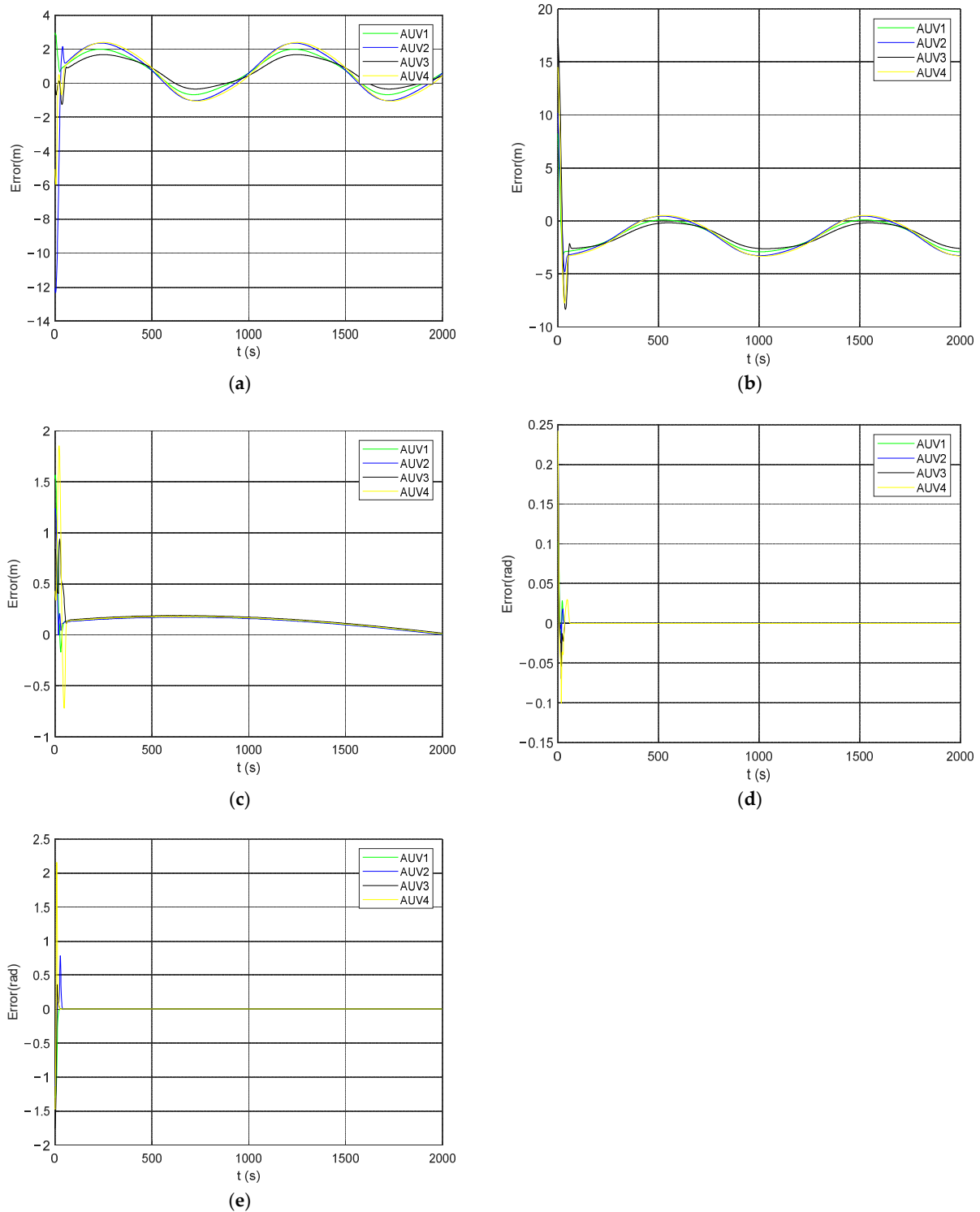
Figure 14. Errors of follower AUV under CNN-LSTM model prediction: (**a**) northward error, (**b**) eastward error, (**c**) vertical error, (**d**) longitudinal inclination angle error and (**e**) bow angle error.
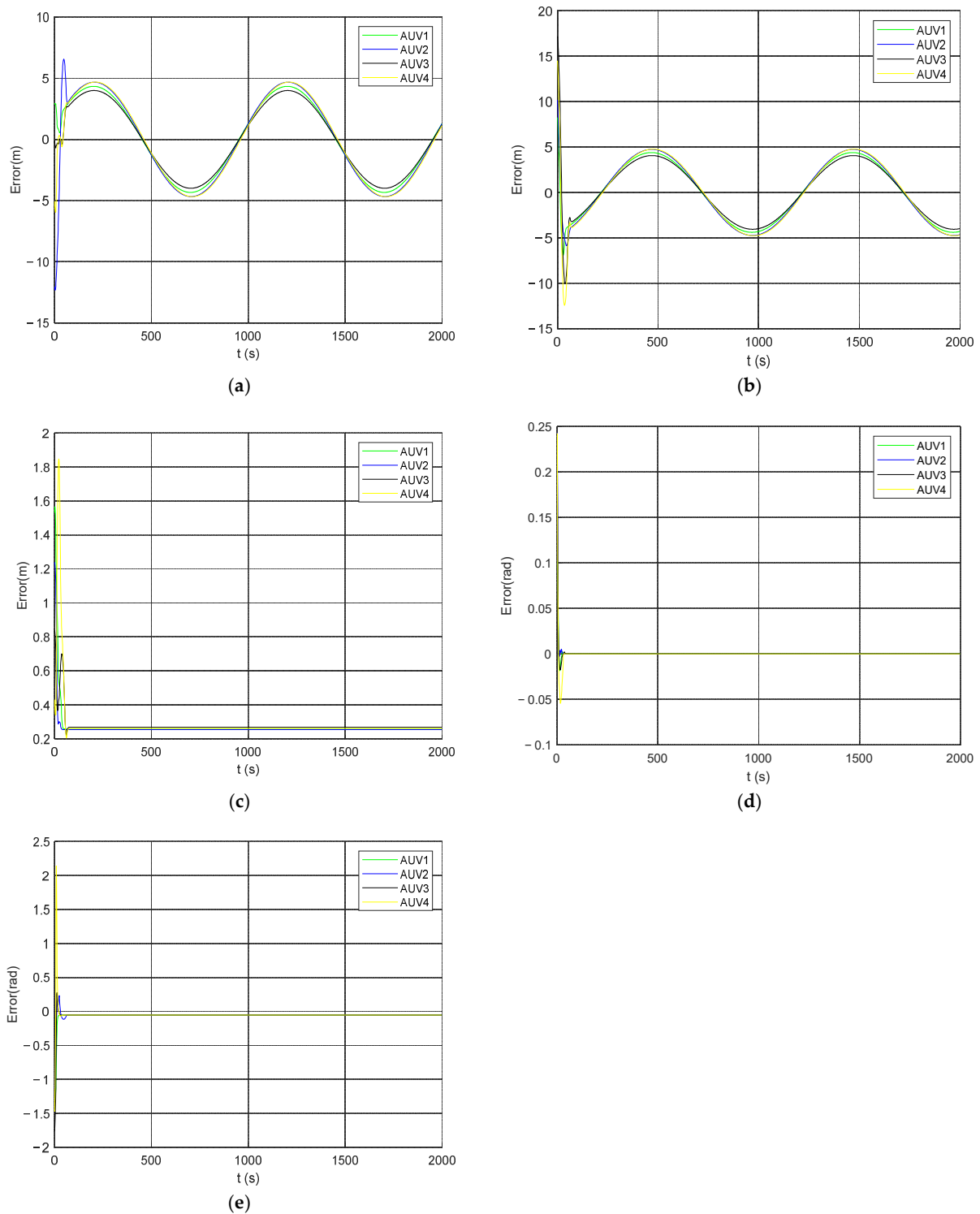
Figure 15. Errors of follower AUV under time delay: (**a**) northward error, (**b**) eastward error, (**c**) vertical error, (**d**) longitudinal inclination angle error and (**e**) bow angle error.

6. Conclusions

This paper focuses on the multi-AUV formation control problem under communication constraints. Firstly, a five-degree-of-freedom nonlinear model of the AUV is established and processed by using feedback linearization to obtain a second-order integral model of the AUV. A sliding-window-based formation prediction control strategy is designed to iteratively predict the current state information of the leader by the historical state informa-

tion of the leader step by step. The method saves computational efficiency and has better adaptability. The CNN-LSTM prediction model is chosen to predict the trajectory state of the navigator for the characteristics of AUV motion trajectory with certain temporality, which compensates for the influence of communication delay on the formation control; and the backstepping method and sliding mode control are combined to design the formation controller, which improves the robustness of the controller. The stability of the control is proved based on Lyapunov stability theory. The effectiveness of the CNN-LSTM prediction model and the designed controller are verified by simulation.

References

1. Glaviano, F.; Esposito, R.; Di Cosmo, A.; Esposito, F.; Gerevini, L.; Ria, A.; Molinara, M.; Bruschi, P.; Costantini, M.; Zupo, V. Management and Sustainable Exploitation of Marine Environments through Smart Monitoring and Automation. *J. Mar. Sci. Eng.* **2022**, *10*, 297. [CrossRef]
2. Wolek, A.; McMahon, J.; Dzikowicz, B.R.; Houston, B.H. The Orbiting Dubins Traveling Salesman Problem: Planning inspection tours for a minehunting AUV. *Auton. Robot.* **2021**, *45*, 31–49. [CrossRef]
3. Ru, J.; Yu, H.; Liu, H.; Liu, J.; Zhang, X.; Xu, H. A Bounded Near-Bottom Cruise Trajectory Planning Algorithm for Underwater Vehicles. *J. Mar. Sci. Eng.* **2023**, *11*, 7. [CrossRef]
4. Khan, J.U.; Cho, H.-S. Data-Gathering Scheme Using AUVs in Large-Scale Underwater Sensor Networks: A Multihop Approach. *Sensors* **2016**, *16*, 1626. [CrossRef] [PubMed]
5. Liu, H.; Xu, B.; Liu, B. An Automatic Search and Energy-Saving Continuous Tracking Algorithm for Underwater Targets Based on Prediction and Neural Network. *J. Mar. Sci. Eng.* **2022**, *10*, 283. [CrossRef]
6. Chen, T.; Qu, X.; Zhang, Z.; Liang, X. Region-Searching of Multiple Autonomous Underwater Vehicles: A Distributed Cooperative Path-Maneuvering Control Approach. *J. Mar. Sci. Eng.* **2021**, *9*, 355. [CrossRef]
7. Li, J.; Zhai, X.; Xu, J.; Li, C. Target Search Algorithm for AUV Based on Real-Time Perception Maps in Unknown Environment. *Machines* **2021**, *9*, 147. [CrossRef]
8. Mao, S.; Yang, P.; Gao, D.; Bao, C.; Wang, Z. A Motion Planning Method for Unmanned Surface Vehicle Based on Improved RRT Algorithm. *J. Mar. Sci. Eng.* **2023**, *11*, 687. [CrossRef]
9. Chen, Y.; Wu, W.; Jiang, P.; Wan, C. An Improved Bald Eagle Search Algorithm for Global Path Planning of Unmanned Vessel in Complicated Waterways. *J. Mar. Sci. Eng.* **2023**, *11*, 118. [CrossRef]
10. Yan, Z.; Yue, L.; Zhou, J.; Pan, X.; Zhang, C. Formation Coordination Control of Leaderless Multi-AUV System with Double Independent Communication Topology and Nonconvex Control Input Constraints. *J. Mar. Sci. Eng.* **2023**, *11*, 107. [CrossRef]
11. Yu, H.; Zeng, Z.; Guo, C. Coordinated Formation Control of Discrete-Time Autonomous Underwater Vehicles under Alterable Communication Topology with Time-Varying Delay. *J. Mar. Sci. Eng.* **2022**, *10*, 712. [CrossRef]
12. Kang, X.; Xu, H.; Feng, X. Fuzzy Logic Based Behavior Fusion for Multi-AUV Formation Keeping in Uncertain Ocean Environment. In Proceedings of the OCEANS 2009, Biloxi, MS, USA, 26–29 October 2009; pp. 1–7.
13. Borhaug, E.; Pavlov, A.; Pettersen, K.Y. Straight line path following for formations of underactuated underwater vehicles. In Proceedings of the 2007 IEEE 46th IEEE Conference on Decision and Control, New Orleans, LA, USA, 12–14 December 2007.
14. Ding, G.; Zhu, D.; Sun, B. Formation control and obstacle avoidance of multi-AUV for 3-D underwater environment. In Proceedings of the 2014 33rd Chinese Control Conference, Nanjing, China, 28–30 July 2014.
15. Li, J.; Zhang, Y.; Li, W. Formation Control of a Multi-Autonomous Underwater Vehicle Event-Triggered Mechanism Based on the Hungarian Algorithm. *Machines* **2021**, *9*, 346. [CrossRef]

16. Chen, Y.; Guo, X.; Luo, G.; Liu, G. A Formation Control Method for AUV Group Under Communication Delay. *Front. Bioeng. Biotechnol.* **2022**, *10*, 848641. [CrossRef] [PubMed]
17. Suryendu, C.; Subudhi, B. Formation Control of Multiple Autonomous Underwater Vehicles Under Communication Delays. In Proceedings of the 2020 IEEE Transactions on Circuits and Systems II: Express Briefs, Goa, India, 28 February 2020.
18. Yang, S.; Chen, J.; Liu, F. Observer-Based Consensus Control of Multi-Agent Systems with Input Delay. In Proceedings of the 2018 IEEE 4th International Conference on Control Science and Systems Engineering (ICCSSE), Wuhan, China, 21–23 August 2018.
19. Liu, Y.B. Research on Coordination Control of Multiple Underwater Vehicles for Ocean Exploratio. Ph.D. Thesis, Harbin Engineering University, Harbin, China, 2017. (In Chinese)
20. He, Y.Y.; Yan, M.D. *Nonlinear Control Theory and Application*; Electronic Science and Technology University Press: Xi'an, China, 2007; pp. 115–119. (In Chinese)